Project no. TIP5-CT-2006-031415O

# INNOTRACK

Integrated Project (IP)

Thematic Priority 6: Sustainable Development, Global Change and Ecosystems

# D4.2.4
# Improved model for loading and subsequent deterioration due to squats and corrugation

Due date of deliverable: 2009-02-28

Actual submission date: 2009-04-17

Start date of project: 1 September 2006 Duration: 36 months

Organisation name of lead contractor for this deliverable: TU Delft

Revision: Final


| Project co-funded by the European Commission within the Sixth Framework Programme (2002-2006) | | |
|---|---|---|
| **Dissemination Level** | | |
| **PU** | Public | PU |
| **PP** | Restricted to other programme participants (including the Commission Services) | |
| **RE** | Restricted to a group specified by the consortium (including the Commission Services) | |
| **CO** | Confidential, only for members of the consortium (including the Commission Services) | |

# Table of Contents

# Glossary

| | |
|---|---|
| CWR | Continuously welded rails |
| DWDPD | Differential wear and differential plastic deformation |
| KMS | Knowledge management system |
| MB | Multi-Body dynamics |
| FE | Finite Element method/model/analysis |
| RCF | Rolling contact fatigue |
| SP | Sub Project |
| WP | Work Package |
| | |
| Chalmers | Chalmers University of Technology, Göteborg |
| DB | Deutsche Bahn Technik/Beschaffung |
| TUD | Technical University Delft |
| VAS | Voestalpine Schienen GmbH |

# 1. Executive Summary

In this research a hybrid multibody-finite element model was developed and applied to the analyses of the initiation and growth of squats, and to the identification of the most influential parameters of squatting. The growth process of squats was postulated based on numerical simulation, and was subsequently validated by field monitoring. Further a critical size for small rail top geometrical defects to grow into squats has been derived and validated. This critical size may be directly applied to visual inspection and classification of squats so that false reporting of squats can be avoided. The critical size can be applied as a minimum action rule for preventive or early corrective maintenance actions, such as rail grinding. The model may also have the capability to relate the severity of some track short defects quantitatively to some measurement of the dynamic wheel-rail interaction at the defects so that automatic detection of the defects at their early stage is possible. Finally corrective and preventive measures against squats are discussed.

# 2. Introduction

The overall objectives of Work Package (WP) 4.2 are (see the INNOTRACK Description of Work):

- To evaluate tolerances and limits for rails and joint degradation in terms of allowable magnitudes of wear, corrugation, geometrical deviations, etc under different operational conditions.
- To establish minimum action rules for the occurrence of material defects under different operational conditions and rail/joint degradation

This deliverable is a step towards these objectives.

To further detail the contributions of WP 4.2 and its interaction to other Sub-Projects (SP) and WPs, it was clarified at the WP 4.2 meeting 15th of February 2007 that the focus in WP4.2 is mainly on vertical train–track interaction and related. In addition longitudinal forces due to braking/traction will be included when suitable. Analysis of lateral train–track interaction and subsequent deterioration calls for vehicle models that are largely lacking or are not available for use in INNOTRACK. This topic is therefore left for the low- and medium-resolution modelling of SP1. This includes e.g. prediction of the formation of head checks. In addition to SP1, lateral train–track dynamics and subsequent deterioration will also to some extent be studied in SP3 and WP4.3.

Within these frames, the work within WP4.2 includes the collection of input and validation data and actual numerical simulation and resulting quantifications of increased operational loads and deteriorations.

The current report focuses on two phenomena: squats and corrugation.

In this study the term “squat” denotes singular surface indentations. To get a firmer confirmation how these relate to other reports of “squats” found in the literature a more in-depth metallographic examination is needed. Though an important issue, it is considered outside the scope of the current study where we focus on the influence of the surface indentations (“squats”) on induced contact forces and subsequent “squat” growth.

Further corrugation is studied with respect to its influence of vertical contact force magnitudes and induced rolling noise. Corrugation may lead to other unwanted phenomena, but these two were consider the main concerns and thus selected for an in-depth analysis.

# 3. Input data gathering

- Stress–strain curves for 260 and 350HT (Corus and VAS)
- Measured dynamic receptance of track at singular irregularities
- Vibration and frequency characteristics of the vehicle-track system related to the contact forces at singular irregularities
- Measured singular irregularities, especially geometry and crack depth of squats and belgrospis (high speed line) (DB)
- Measured rail top geometries (longitudinal) at insulated joints and welds (ProRail)

# 4. Loading and deterioration of squats

## 4.1 Introduction

### 4.1.1 Literature review

Squats were first reported in the 1950s in Japan where it was described as the 'black spot' [1, 2, 3]. In the 1970s they became known in the UK [4]. In other European countries they were reported later [5, 6]. A definition of squats can be found in [7]. Squats have in recent years become an important rolling contact fatigue (RCF) problem for railways, such as ProRail [6, Annex 1].

Researches on squats have been carried out over the past decades. In [8] Clayton presented a research programme of the British Rail Research, the goal of which was to develop a failure model based on small scale laboratory test; some results were reported in [8] and [9].

In 1987 the European Rail Research Institute (ERRI) started the D173 Rolling Contact Fatigue Programme, an overview of which can be found in [10]. Squats were investigated in this programme; some of the results were summarized by Cannon and Pradier [10]. The major work on squats was on crack growth; it was presented by Bogdanski *et al* [11]. Bogdanski and his colleagues have since then published a series of work related to cracks of squats, especially in relation to fluid entrapment, with the latest being [12].

Kondo *et al* [13] presented the history of the Shinkansen rail surface shelling, which was also squats in Japan, and discussed the causes, growth and detection; Grinding was the countermeasure. Some recent work on the squats in Japan was reported by Ishida *et al* [14], in which the initiation mechanism and the effect of grinding were discussed. Other works on squats can be found in [15 - 18].

It is noted that the definition of squat may differ in certain degree at different time and in different railways. For instance "in the UK, the RCF defects were classified as squats" in the late 1990s, according to Cannon *et al* [22].

### 4.1.2 Definition of squats employed in this deliverable

In this report the definition of squats of UIC712R [7] (defect type227) is used. The characteristics of squats, according to [7] are: Squats is visible on the rail head as widening and a localised depression of contact surface, accompanied by dark spot containing cracks with circular arc of V shape. The cracks propagate inside the rail head, at first at a shallow angle to the surface. Then when they reach 3 – 5 mm depth, they propagate downward transversely.

The definitions of squats of the NetworkRail [19] and ProRail [20] are in agreement with that of [7], but with more details. For instance the visible cracks may also be U, Y or horseshoe shaped. But the most significant is that the squats bear the shape of two lungs, see Figures 1 and 3 for examples. The shape of two lungs may be disturbed and less obvious when a squat is severe and there are many visible cracks, for instance with the one in Figure 4.

In [19] hypotheses of squat formation are presented. It is mentioned that squats may be caused by periodic indentations. But such indentations are not called squats in [19]. The hypothesis of [19] relates squats formation with cracks, and stated that "'normal' squats develop for much the same causes as head checks".

In contrast to [19] small rail top geometrical defects (See Figure 2 for examples), if large enough, are explicitly classified as light squats in [20]. They are sometimes also called early squats, or squats seeds. This classification is based on many observations of the Dutch railway that such defects will grow into a typical matured squat like those of Figures 1, 3 and 4. This classification facilitates early identification of (light) squats, so that low life cycle costs can be realized through timely maintenance. Figures 3 and 4 show two matured Dutch squats. They clearly bear all the characteristics of squats mentioned above.

(a) A squat from [19] (b) A squat from [20]

Figure 1, Two typical squats of NetworkRail (a) and ProRail (b).

The hypothesis of [19] seems not able to explain the formation of most of the squats in the Netherlands. In particular in the process of light squats growing into moderate squats cracks appear not necessarily to be an important factor. Rather it seems, based on the correlation analyses, that the high frequency dynamic rolling contact seems more dominant. Such dynamics is not present in the hypothesis of [19].

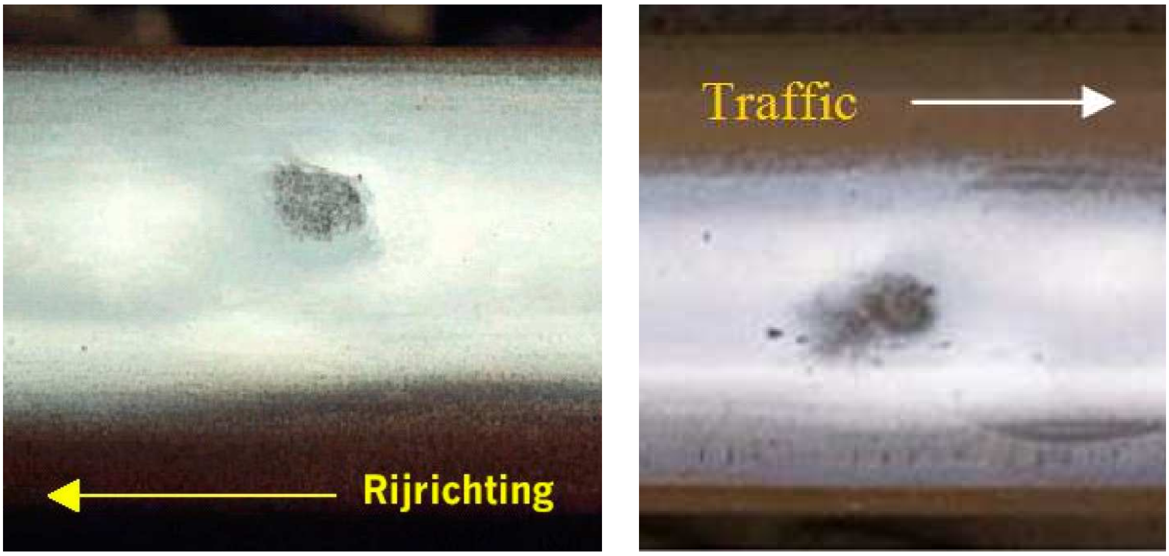


(a) Taken from [20] (b) Taken from annex [3]

Figure 2, Examples of light squats according to ProRail classification (From [20]).

### 4.1.3 Focus and hypothesis of this deliverable

It is obvious that squats such as shown in Figures 1 and 3 must have grown from something small. Such small things can be periodic indentations [19] or other rail top geometrical defects [20]. From infra management point of view, it is most cost effective if squats can be removed from the rails by grinding at their early stage. This deliverable focuses, therefore, itself on such small defects, which, for convenience of reference, are called light squats hereinafter. In particular the focuses will be: How light squats grow into matured squats of the characteristic two-lung shape, and what is the critical size to distinguish light squats from trivial defects.


*(a) The squat*

*(b) The cross-section of the broken squat*

Figure 3, A squat with a maximal crack depth of 3.5mm. The drawing at the lower right corner of (a) shows schematically the visible shape of the cracks. (b) shows the cross-section broken by four-point bending.


*(a) A severe squat*

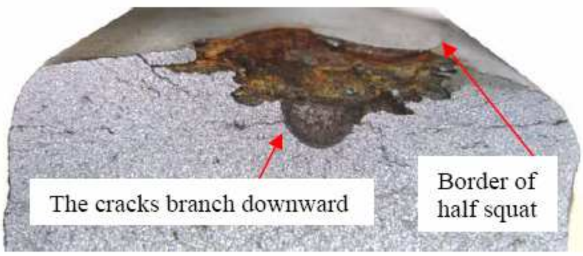


*(b) Cross-section of the broken rail at the squat*

Figure 4, A squat with a maximal crack depth of 10.5mm. (b) shows the cross-section broken by four-point bending. The crack branches down.

**Definition of light squats**

In general, light squats can be any small rail top geometrical defects which can cause sufficiently large high frequency wheel-rail interaction (impact). In the light of this definition the defects can be indentations, short pitch corrugation, small wheel burns, cracks, etc.

Rail top geometric deviation due to differential wear and differential plastic deformation (DWDPD) can also be sources of squats. DWDPD may occur at welds due to their material inhomogeneity in the hit affected zone (HAZ). This is why in [7] and [19] welds are mentioned as a source of squats. It is noted that defects in the track structure may cause DWDPD as well. Corrugation may be considered as a result of DWDPD due to defective track because it is caused by repeated wear or plastic deformation which differentiates from place to place. While DWDPD of corrugation is periodic over a length of rail, singular DWDPD may occur at places of such as sudden stiffness changes at fish-plated joints and at switches and crossings (S&C), when the joints or S&C are accompanied by other defects. An example is given in section 4.4.4.

**Hypothesis of this deliverable**

The hypothesis of this deliverable is that squats grow from small rail top defects due to the geometrical deviation which cause sufficiently large high frequency (short wave) wheel-rail interaction. The dynamic contact force causes accumulation of plastic deformation, so that the defects grow due to rachetting [21] into typical matured squats, in a process like positive feedback – the dynamic force causes growth of the defect and vice versa. The criterion for surface plastic deformation to take place is that the von Mises stress exceeds the yield strength of the material. The yield strength increases with hardening, until the tensile strength is reached.

The defects do not necessarily need to have cracks in the beginning. This is evidenced by the fact that indentations, corrugation, welds and DWDPD usually do not have cracks in the beginning. The cracks of squats are a consequence of the exhaustion of the material ductility or fatigue resistance. Hence cracks are not considered in this deliverable because of its focus. It will be shown in annexes 1 and 3 that this omission does not affect the findings and conclusions of this deliverable, i.e. mainly the process of light squats growing into the typical matured squats of the characteristic two-lung shape with a wavelength between 20 – 40 mm, the critical size for distinguishing light squats from trivial defects, and the signature tunes for early detection of squats by measurement of dynamic response. The cracks, when they are not very deep, have only effects in their vicinity, while the dynamic interaction, which is the basis of all the conclusions, is related to the local wheel-track system.

This deliverable attempt to answer the following questions to support the hypothesis:

- What is the critical size for small defects to grow into squats? This critical size can then be the criterion to distinguish between light squats and trivial defects.
- How does a light squat grow into a matured typical squat of the characteristic lung-like shape?

By answering these questions, the loading conditions for squats to initiate and grow can be clarified; the parameters in the vehicle-track system which may influence the initiation and growth of squats can be identified. Subsequently, possible methods may be proposed for early detection of squats and some of the influential parameters; maintenance criteria and counter measures for low LCC can be derived and proposed.

The hypothesis implied a major difference between the initiation and growth mechanisms of the two main rail RCF types: squats and head checking (HC, including gage corner checking): For squats, it is a dynamic process of high frequency wheel-rail interaction, while for HC, it is a (quasi-) static process. It is noted that at the late stage of HC, when its sub-surface cracks extend to the middle of the rail head, high frequency wheel-rail interaction can as a result be excited, so that the HC may grow into a superficial appearance like a matured squat.

The difference between this work and previous work lies mainly in that here dynamic interaction plays a major role; cracks and metallurgical aspects are not taken into account. It does not mean that these two aspects are not important. Rather it is the cracks which make squats dangerous. And metallurgy and microstructure of the rail materials may play a significant role in the formation and growth of squats. But due to the limited duration of the project and the focus on early action, the present treatment has been opted.

### 4.1.4 Approach of this deliverable

The approach of this deliverable is a combination of field observations and monitoring, and numerical modelling. In the first place correlation and statistical analyses of field observations were carried out to gain global and physical insight into the relation between squats and track parameters. This led to the conclusion that squatting is strongly related to local high frequency wheel-rail interaction, with influence from local track system such as fastening and rail pads. Subsequently a transient Finite Element (FE) model was developed to simulate such dynamic wheel-rail rolling contact at defects of various sizes. Finally field observations and measurements are shown to prove the validity of the numerical results.

It would be ideal if validation of the numerical results by controlled laboratory test could be included in this report. But that is impossible at this moment for the results obtained so far.

It is noted that the analyses are performed in this deliverable for typical Dutch railway cases. The procedure and the model used are applicable to other railways.

### 4.1.5 Outline of this deliverable

Following the approach described above, this deliverable first presents briefly in section 4.2 the correlation analyses, which highlight the dominant role of rail top defects and the important roles of the local track structure, friction and material properties. As a consequence the FE model of Section 4.3 is focused on the modelling of the transient frictional rolling contact at the defects, with the local track system being properly taken into account.

Now that the most influential factors for squats to occur have been narrowed down from the correlation analyses and the corresponding FE model has been built up, the model is applied In Sections 4.4.1 – 4.4.3 to determine the critical size, above which the chance for a rail top defect to grow into a typical squat is large. The critical size is validated by filed monitoring. In Sections 4.4.4 a squat at the end of a fishplate is analyzed to show how DWDPD may occur at sudden change of stiffness, accompanied by other defect in the track, in this case the loose fishplate bolt. Section 4.4.5 shows that the DWDPD causes increased contact force, both in the normal and in the tangential (longitudinal) directions.

Next in Section 4.5.1 based on numerical modelling a growth process is postulated for a light squat to grow into a typical squat with the characteristic two lungs. The validation of the numerical of Section 4.5.1 and Annex 1 is presented in Section 4.5.2, with much more details in Annex 3.

Section 4.6 discusses the influence of the vehicle and track parameters on squat initiation and growth, and Section 4.7 presents some preliminary results of forces and stresses in railpad, sleeper and ballast caused by large squats.

Finally counter measures are discussed.

## 4.2 Correlation analyses

Correlations of squat occurrence with some factors and parameters in the vehicle-track system have been established based on analyses of measured track geometry data and field observations of the Dutch

Railways [23].

It is concluded that squat occurrence can be related to track short wave irregularities, especially on the rail top such as indentations, weld and corrugations. Material strength, un-sprung mass, traction and braking, sleeper spacing and fastening system properties also play important roles.

## 4.2.1 Correlation with track structure parameters

Correlation was identified with short wave irregularities. It was found that about 74% of the squats were on the ½ rails centered on sleepers and the rest were on the other ½ rails centered between two sleepers, see figure 5. This suggests that the stiffness and damping characteristics of the track, particularly those of the rail and the rail pad, and their technical status may have played a role.

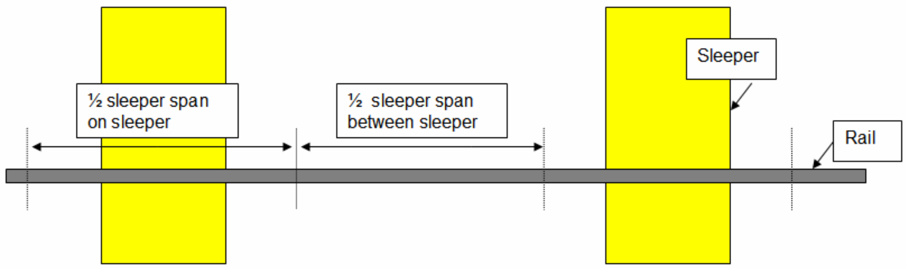


*Figure 5, Definition of the half sleeper span centered on sleepers and the other half between sleepers.*

It was also found that short pitch corrugation with various severities could be seen in the neighborhood of about 72% of the squats, with a wavelength ranging between 2 and 6 cm. Later a numerical analysis (annex 1) showed that the growth of a squat is accompanied and promoted by a dynamic wheel-rail interaction force, which is excited by the squat itself, and which has the wavelength of short pitch corrugation. This suggested that for the corrugation seen in the neighborhood of the above mentioned 72% of squats, some might not really be corrugation, but could be wave patterns of the un-uniform plastic deformation or wear caused by the dynamic contact force. The available data were, however, not suitable for proving such a proposition, because the traffic directions were not known. Another field survey was therefore subsequently conducted; it confirmed the proposition: in total 74% of the investigated squats had short pitch corrugation-like rail surface waves around them, among which 33% was indeed short pitch corrugation, which means that the waves are simultaneously before and after the squats. For the other 41%, the wave pattern was found only after the squats, see figure 6 for illustration. For all the investigated squats in the second survey the wavelength of the wave pattern was again in the range of that of the short pitch corrugation.

The similarity of squats and short pitch corrugation in their wave pattern has some significance. The squats found at corrugation should have initiated directly from the rail surface irregularity of the corrugation. The other 41% should have initiated from other sources, the wave pattern following them being the consequence of the dynamics force excited by them. In both cases the wavelength should have been determined by the eigen characteristics of the local wheel-track system. In view of the similarity in the wavelengths of the corrugation and the wave pattern, the eigen systems for the occurrence of short pitch corrugation and of the squats wave pattern should have some characteristics in common.

These statistics are largely in line with a investigation of the UK: according to historic research 75% of squats are associated with one of the following features: corrugation, welds and periodic indentations in the rail running surface caused by hard objects brought forward by the wheels [19].

Relation of squat occurrence with track irregularities such as alignment, cross level, gauge and vertical profile was analyzed; effects of rail vertical wear and rail foot inclination were examined. There was no clear correlation found, as was expected, because these measurements are of the long wave type, with a resolution of 25cm.

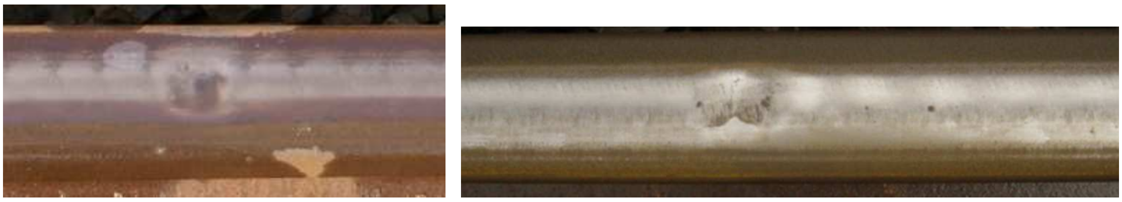

*(a) Corrugation causes squats* *(b) Squat causes corrugation-like wave pattern*
*Figure 6, Short pitch corrugation and corrugation-like wave pattern after a squat. Their wavelength is usually in the range of 2 – 6 cm. Traffic from left to right.*

## 4.2.2 Correlation with welds and materials

Out of different field surveys it was found that about 10 – 15% of squats were at welds. Figure 7 shows two typical cases. The vulnerability of welds, both thermite and flash butt, to squatting, may be explained by two reasons: material inhomogeneity in the heat affected zone and geometry deviation.

Figure 8(a) illustrates the hardness distributions of thermite and flash butt welds. Part, if not all, of the weld and the heat affected zone have lower hardness than the parent material. Comparing Figure 7 with Figure 8, resemblance can clearly be seen between the damage, the hardness variation and the rail top longitudinal profiles. Obviously the hardness difference in the heat affected zone will lead to variations in plastic deformation and wear behavior. This local un-uniform deformation and wear, when accumulated after repeated wheel passages, may cause significant increase in local dynamic contact force, which in turn result in further differential deformation and wear, like a positive feedback. If there is already geometrical deviation due to imperfect grinding after welding, the problem will be exacerbated.

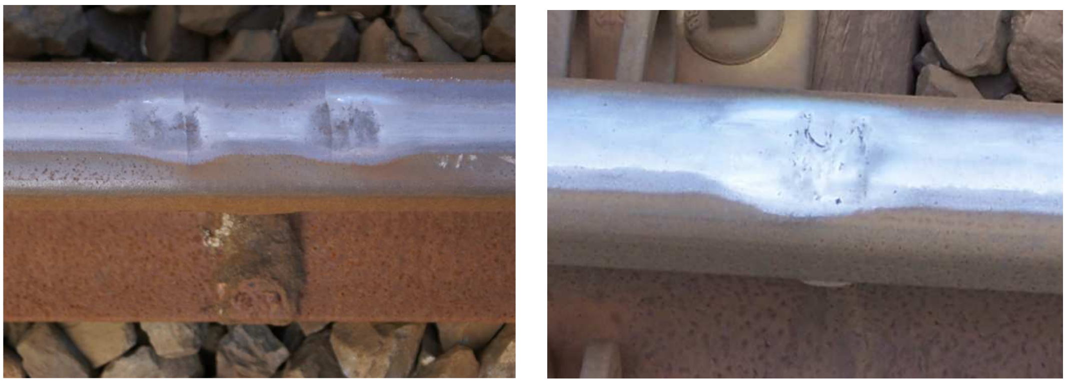

*(a) A squat at a thermite weld* *(b) A squat at a flash butt weld*
*Figure 7 Squats at welds*

## 4.2.3 Correlation with rail surface irregularities

In nature squats are visually rail top geometry deviation due to large plastic deformation. They must therefore grow from some small rail top irregularities. These can be

- Indentations by hard alien objects between wheels and rail. They can be, for instance, a hard ball from an aerosol paint can, or a ball or roller from a bearing. They can indent into the wheel and be brought forward. Such indentations can be recognized by their periodicity of the wheel circumference of usually about 3m.
- Vertical mis-alignments of the rails, e.g. at switches and crossings.
- Short pitch corrugation.
- Skidding and sliding damages by wheels during traction and braking. This has to do with the low adhesion due to contamination on rail heads, with the high traction power of modern motorized

passenger cars and locomotives, and with the characteristics and performance of their traction control systems and Anti-lock Brake Systems, which allow large slip. Wheel burns can often be observed at and near stations, but also elsewhere.
Sometime wheel burns were made distinct from squats by some authors. In this chapter they are considered as an initiation source of squats because defects developed from wheel burns in the later stages bear all the characteristics of squats. Figure 9 shows such an example.

- Differential wear and differential plastic deformation.
Rails experience inevitably wear, and often also plastic deformation. These wear and deformation are usually uniform along the rails. If, for some reasons, un-uniform local wear or plastic deformation takes place repeatedly at fixed places and accumulate, differential wear and deformation occur. Welds, due to their heat affected zone and poor finish geometry, can often have such wear and deformation, as is discussed above. Short pitch corrugation, with its damage mechanism being plastic deformation and wear [24], may also be of the type of differential wear and differential deformation which repeat itself over a long length of rail. The wave pattern following a squat discussed above is also due to differential wear and plastic deformation caused by the dynamic force excited by the squat itself.
Poorly laid or maintained tracks have short defects in the rail, railpad, fastening, sleepers and support of sleepers etc. They may excite dynamic contact force of the necessary wavelength repeatedly at the same location so that differential wear and plastic deformation occur. Such wear and deformation, when accumulated to certain amount, becomes sources of squat initiation. One of such cases is presented in section 4.4.4 below.

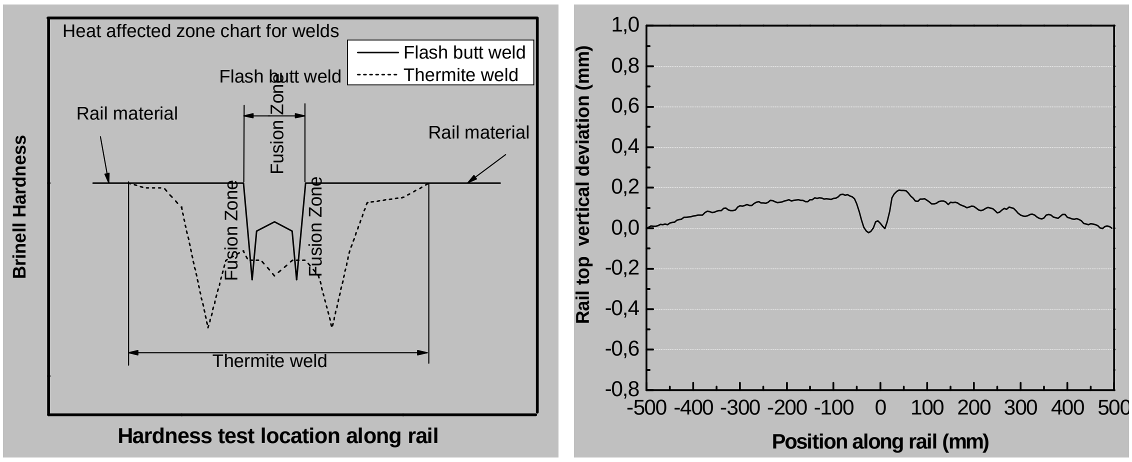


(a) (b)

*Figure 8, Hardness (a) and geometry (b) variations at welds*

## 4.2.4 Correlation with friction

There have been observations which show that squat occurrence is much higher at locations of high traction and braking efforts. Statistics of a European railway show significant increase in squats occurrence at ascending gradient of higher than 1%.

# 4.3 The numerical models

A hybrid transient Multi-Body-Finite-Element (MB-FE) approach has been taken, see figure 10 for the model. Details are given in annexes 1 and 2. The advantages are

- The rail and the wheel are modelled with three-dimension FE mesh in the area of interest, detailed stresses and strains in the contact area and in the bulk materials can be studied.
- The parts farther away can be modelled with coarse mesh or with rigid body, where appropriate, so that the effects of the vehicle and the track can all be simultaneously taken into account, with affordable

computing costs.
- The short wave/high-frequency dynamical characteristics of the problem can therefore be fully taken into account in the calculation of the stress and strain states. Wave propagation in the continua is also accounted for.
- Friction is considered in the contact. Therefore not only the dynamic vertical force, but also the dynamic tangential force and the associated creepage is fully accounted for.
- Non-linear material properties, such as plasticity, can be taken into account. Material behaviour under high hydrostatic pressure can also be modelled.
- Arbitrary contact geometry can be modelled.

*Figure 9 A squat developed from a wheel burn*

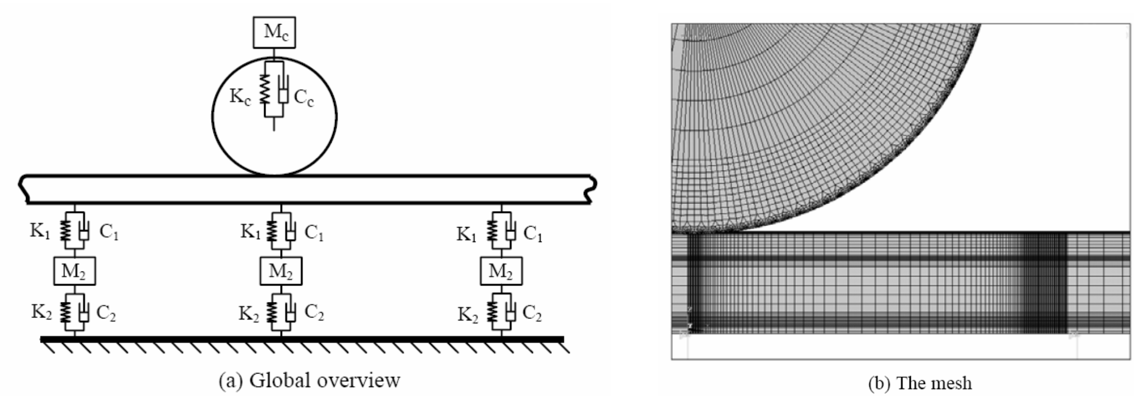


*Figure 10 The hybrid MB-FE model*

The model (annex 1) and its extension (annex 2) have been validated in the following aspects:

- Calculated wavelength of contact force is in agreement with that of the wave pattern following squats, observed in the field, see annex 1.
- Results in contact force, stress and strain levels, and their positions show good correspondence with field observations, see annex 1.
- The numerically postulated process of squat growth is validated, see section 4.5.2 and annex 3.
- The numerically determined critical size for indentation etc to grow into squats is validated, see section 4.4.3 and annex 4.
- Analysis of squat initiation due to different wear and different plastic deformation is in good correlation with field observation, see annex 2.
- Contact area and pressure are validated against Hertz results in the quasi-static state, see [25].
- Calculated residual stress is in agreement with measurement, see annex 5. (Note that there is a typing error in annex 5: the traffic direction of Figure 1 should be from left to right)

## 4.4 Squat initiation

The major squat initiation causes have been discussed in section 4.2. This section shows by way of numerical simulation how squats may initiate due to some of the causes – indentations, differential wear and differential plastic deformation. Validations of the numerical analyses are also presented.

### 4.4.1 Initiation from indentations – a critical size

Many squats initiate from small indentations. But only those indentations which are larger than certain critical size can grow into squats. The motivations for the determination of a critical size are therefore twofold: it provides a criterion for the evaluation of risk for squats to occur, and it may form a basis for minimum action for squat prevention.

Squats grow always from small rail surface defects, no matter what their root causes are. Currently the best way to remove rail surface defects is grinding. The more severe the squats, the deeper the damaged rail top layer, and the deeper the layer to be removed.

In practice there is so far not yet an effective automatic detection method to find early squats. Therefore IM's are still relying on visual inspection. There is still no quantitative criteria for visual inspection to determine what is a light squat in the Netherlands. This leads of to many fault statistics report of light squats.

In view of these, a critical size for rail surface defects to grow into squats is first determined numerically, using the approach presented above. This critical size is subsequently validated with monitoring data.

### 4.4.2 Derivation of the critical size

The derivation is presented in annex 4.

### 4.4.3 Validation of the critical size

Validation of the derived critical size is presented in annex 4.

### 4.4.4 Initiation from differential wear and plastic deformation

Differential wear and differential plastic deformation have been mentioned as one of the major initiation sources of squats. This section discusses by a case study how such wear and deformation can occur.

It has been observed frequently that at locations of stiffness change in the tracks squats can be found, such as at end of fishplates and in switches and crossings (S&C). Figure 11 shows such an example. Obviously stiffness change should not be the only cause; otherwise there will be squats in almost every S&C and at each fish-plated joint. There should be other influential factors behind.

*Figure 11 A squat at the end of fish-plate. The traffic is downwards.*

The squat in Figure 11 provides a good case for study. A transient FE model was employed (annex 2), as shown in Figure 12. The fish-plates were pressed against the rails by the pre-load of the 4 bolts numbered 1 to 4 in Figure 12(a). Contact and friction were defined at the interface between the fish-plates and the rails. A wheel rolled on the rail at a speed of 140km/h, a typical line speed on the Dutch railway network. Parameter variation analysis was performed with different ballast and fastening stiffness and damping, and different fish-plate bolt pre-load. It was found that it was the fish-plate pre-load condition which played the most important role.

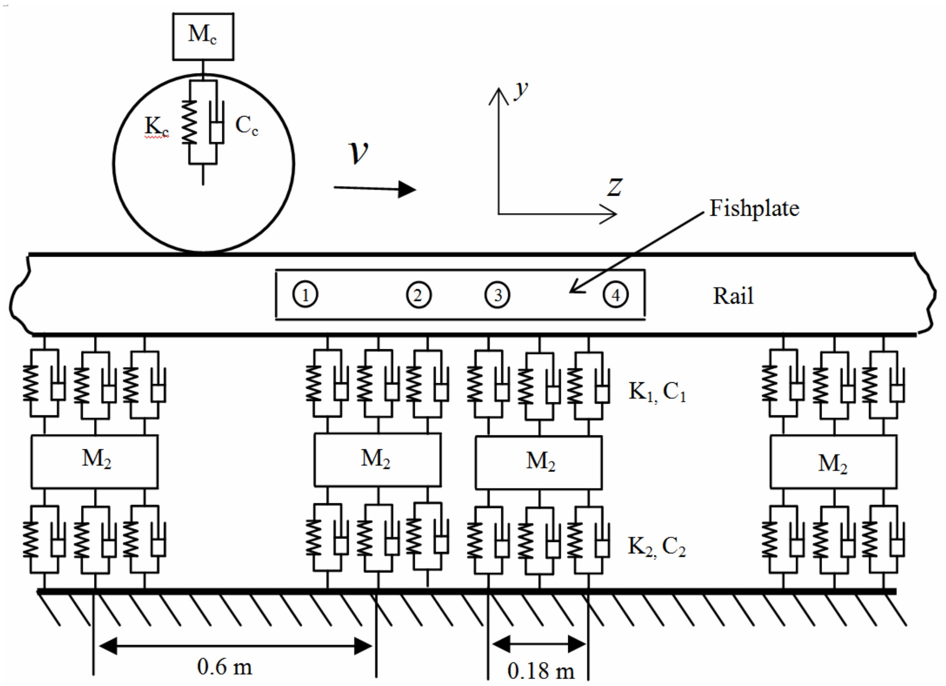


*(a) The overall model*

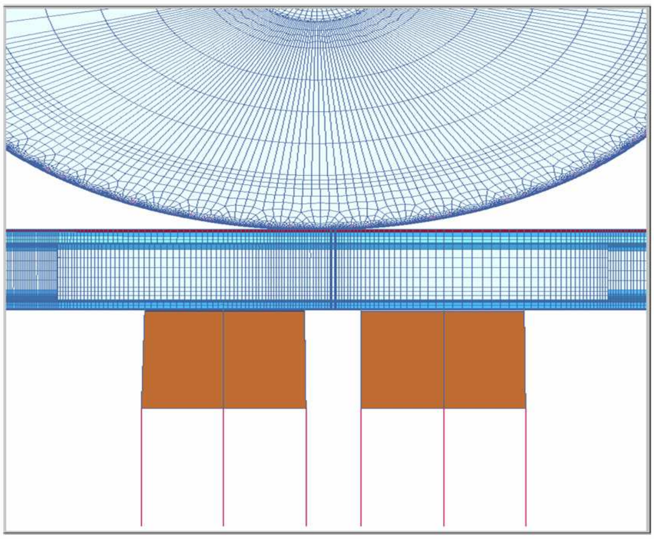

*(b) Zoom-in of the wheel-rail model*

*Figure 12, FE modeling of a wheel rolling over fish-plated rails. The wheel, rail, fish plates and sleepers were modeled as continuum. Other elements in the system were modeled as massed, springs and damper (annex 2).*

Figure 13 shows the vertical and longitudinal contact forces under different fish-plate pre-load. They bear the following characteristics: at the fish-plate end the vertical forces are all broader and flatter at the peak than elsewhere. When the 4th bolt is loose, the peaks, particularly which of the longitudinal force, are the highest at the fish-plate end. This means that the stiffness change at the fish-plate end, together with the loose bolt being closest to the fish-plate end, causes at each wheel passage at the same location a larger contact force with a peak of the necessary width. This force causes at this location more wear than in its neighborhood. Differential wear arises as a consequence. If the force is large enough, differential plastic deformation will also occur. The width of the peak is of importance because if it is too narrow with respect to the size of the contact area, differential wear and deformation may actually not be able to take place. The fishplate and the loose bolt fix the wear and deformation at the same location. Without the location fixing mechanism, the wear and deformation will not accumulate because each passing wheel is somewhat different from another in wavelength, phase and magnitude, so that statistically everywhere along the rail the chance is equal for wear and deformation, and the wear and deformation will be uniform.

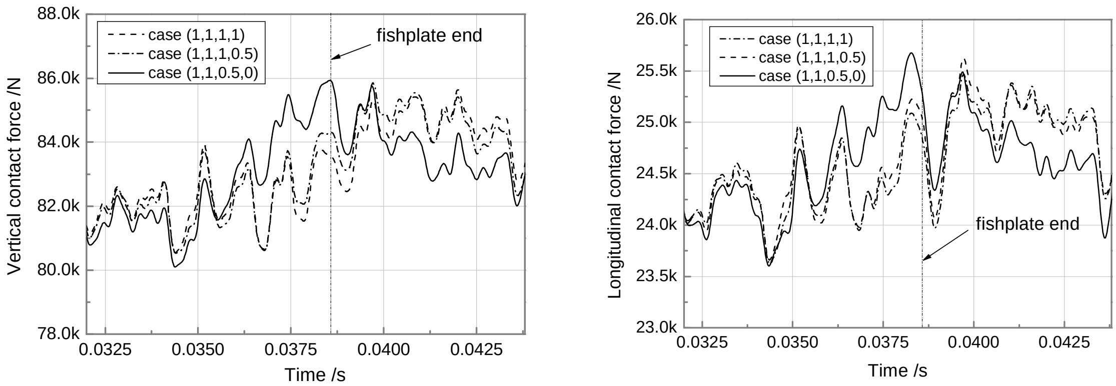


*(a)* *(b)*

*Figure 13, vertical and longitudinal contact forces under different fish-plate pre-loads. (a) Influence of the 3rd and 4th bolt pre-loads on vertical force and (b) the corresponding longitudinal force. Case (1, 1, 0.5, 0) means that at bolts 1 and 2 the bolts were fully fastened, while bolt 3 is half-fastened and bolt 4 is completely loose. The friction coefficient is 0.3 (annex 2).*

The analyzed case shows that one single parameter may not be sufficient to cause a squat. Squats may often be a consequence of the interplay of multiple parameters. This is also confirmed by correlation analyses.

### 4.4.5 Differential wear and deformation cause increased dynamic force

With the accumulation of differential wear and deformation, a small local geometry deviation occurs on rail surface. Such a defect will cause an obvious increase in the dynamic force at the same location, which will further promote wear and deformation.

## 4.5 Squat growth

Rail surface defects due to differential wear and plastic deformation, or due to indentation etc, may grow into squats. In annex 1 the growth of squats was investigated numerically based on the model shown in figure 10, influence of parameters in the vehicle-track system was discussed. A process for squats to grow was postulated, and is summarised in section 4.5.1. In section 4.5.2 and annex 3 the validation of the postulation is presented.

## 4.5.1 A squats growth process is postulated

A squat development process has been postulated based on the correspondence between on the one side the calculated contact force magnitude and its wavelength and on the other side the field-observed squat dimension and the wave pattern following them. The wave length is between 20 – 40 mm. When the traffic speed is about 140km/h, which is typical on the Dutch railway, the frequency is about 1000 – 2000 Hz. It bears resemblance to short wave corrugation.

The postulated squats growth process is as follows (Light squat is called class A squat, and squat A for short; Moderate squat is called class B squat, and squat B for short):

(1) **For a class A squat growing into class B:** As is shown in figure 14, with proper size, position, track and traffic conditions,

a. A typical squat A will has a first impact with a passing wheel at $B_1$ of (b) (i.e. $B_{1G}$ of (a)), causing a peak contact force $B_1$ of (c). This peak force after many wheel passages turns point $B_1$ of (b) into $B_2$ of (d).

b. Then a second peak force $C_1$ of (c) follows. This peak force first causes the wave $B_1C_1$ of (b) in the early stage of the squat-A-growing-into-B process, and then gradually turns wave $B_1C_1$ into the large plastic deformation between $B_2$ and $C_2$ in (d). This is to say that in such a process the part of rail top surface between $B_1$ and $C_1$ in (b) deforms gradually into part of the squat (the part between $B_2$ and $C_2$ in (d)).

c. In the process of turning wave pattern $B_1C_1$ into part of the squat, there may be for certain period no wave pattern after (i.e. to the right of) $C_2$ in (d), because the force peak $D_1$ may not yet be large enough to make a new visible wave pattern.

d.

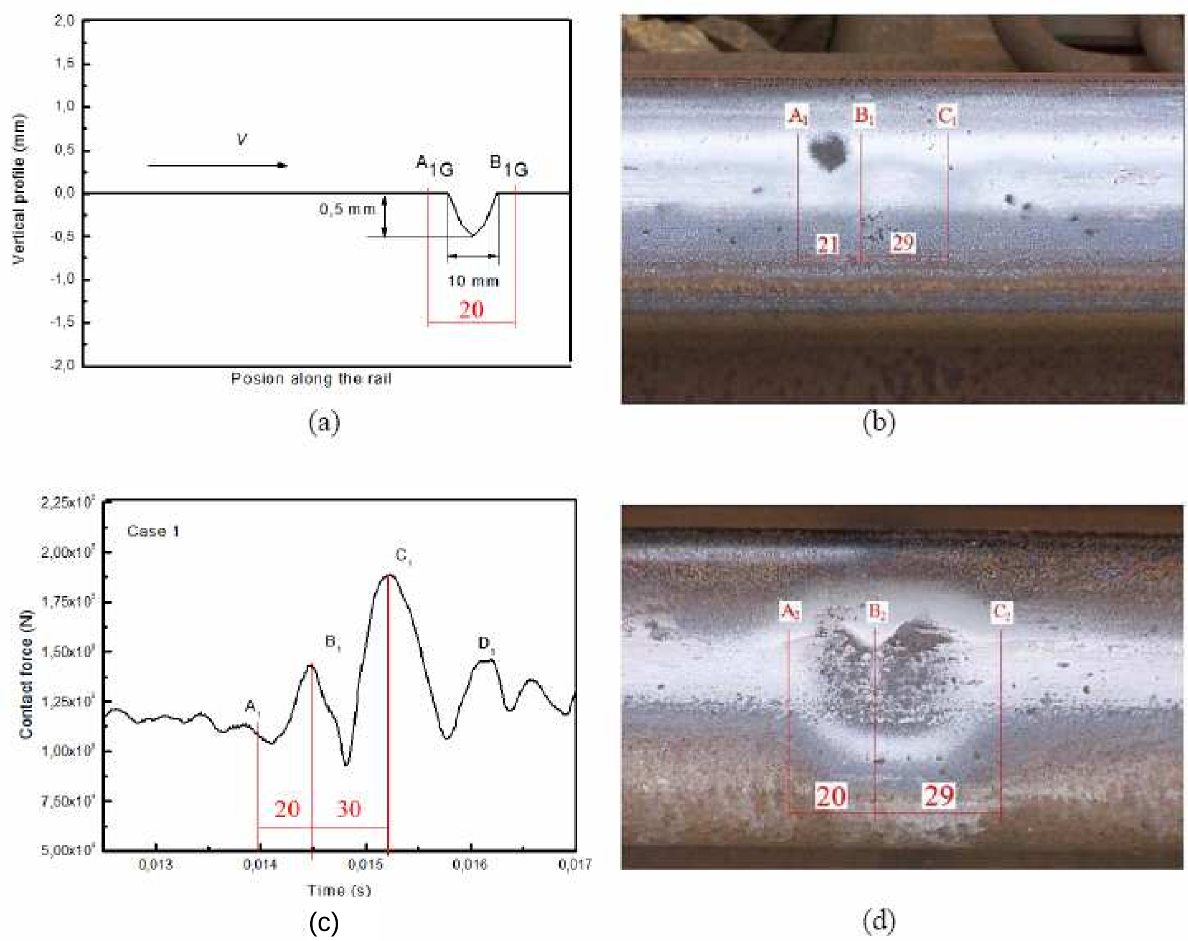


***Figure 14 How a class A squat grow into class B***

Traffic travels from left to right.

(a) Geometry of typical squats A used for the FE model, one of such is shown in (b);

(b) A typical squat A with typical wave pattern after it due to dynamic contact force shown in (c);

(c) The calculated contact force caused by the geometry of (a). Notice that peak $B_1$ is a forced vibration, while peaks $C_1$ and $D_1$ are free vibration

(d) A typical squat B

The red numbers indicate the distances (mm) between the A, B and C points. Subscripts 1 and 2 designate the 2 squat geometries simulated. Subscript G indicates that it is the points on the simulated geometry. Note that the squats in (b) and (d) are two different squats.

Notice the similarity between the wave patterns of (b) and (c), it is postulated that $A_1$ of (b) is $A_2$ of (d), while $B_1$ becomes $B_2$ and $C_1$ becomes $C_2$.

(2) **For a class B squat growing into class C:** As is shown in figure 15,

a. The squat B, together with other track and traffic conditions, causes large impact force so that the squat grows into class C. Wave patterns such as $D_2$ develop after $C_2$.

b. When a squat C develops further, the wave patterns marked with $A_2$, $B_2$, $C_2$ and $D_2$ may be wiped out by the large impact force.

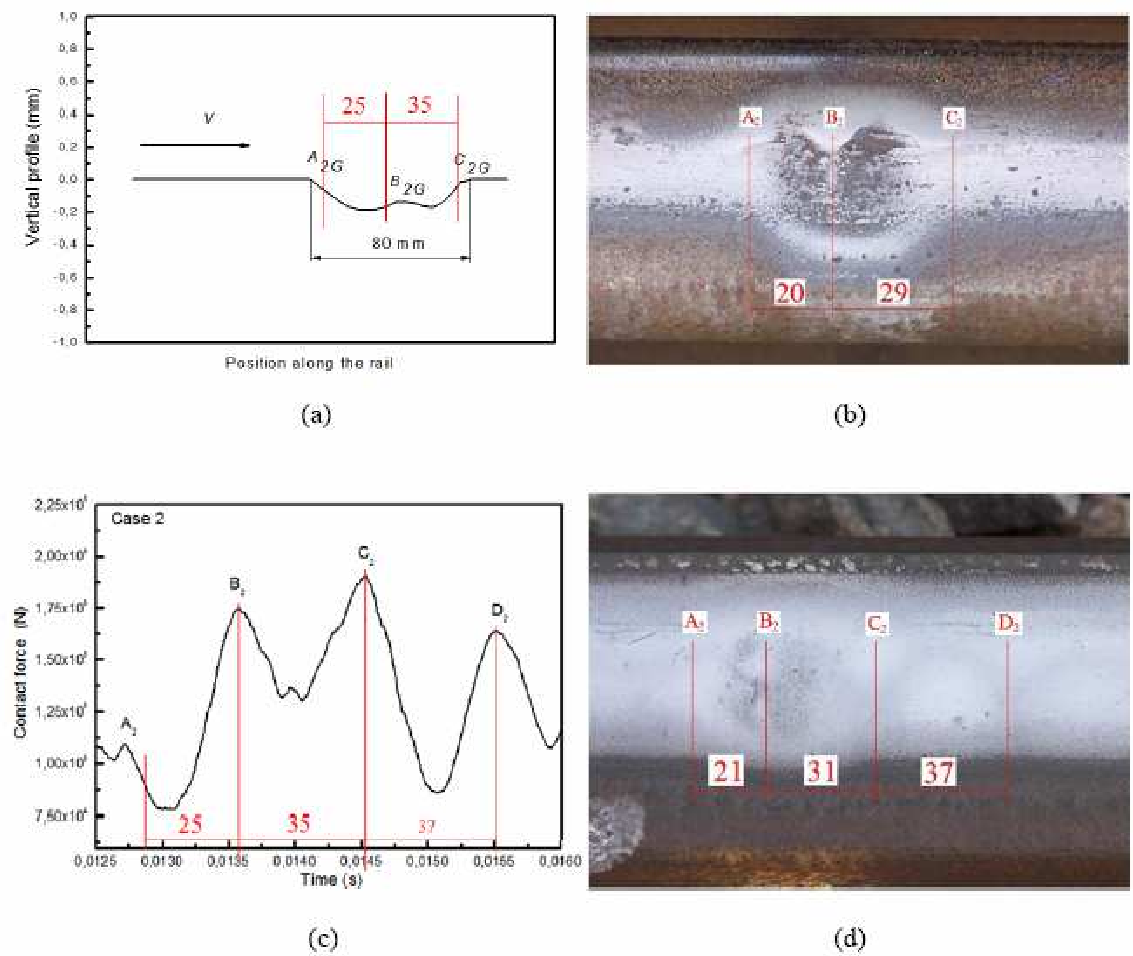


***Figure 15 How a class B squat grow into class C***

Traffic travels from left to right.

(a) Geometry of typical squats B and C used for the simulation, as shown in (b) and (d);

(b) A typical squat B (it is the same as (d) of figure 14);

(c) The contact force caused by the geometry of (a). Notice that the wavelength between $A_2$, $B_2$ and $C_2$ of (c) follows the geometry of (a), as it should be in a forced vibration, while the wavelength $C_2$-$D_2$ of (c) is free vibration;

(d) A typical squat C with typical wave pattern after it due to dynamic contact force shown in (c);

Convention is the same as figure 14. Note that the squats in (b) and (d) are two different squats.

Notice the similarity between the wave patterns of (b), (c) and (d). Compared with (b), (d) has now a new wave $D_2$ after $C_2$, caused by the larger peak force $D_2$.

The small discrepancies between the wavelengths in (b) and (d), e.g. the different distances between $A_2$-$B_2$, may be explained by the fact that the larger the squat deformation, the larger the dynamic contact force, and therefore the larger wavelength. The fundamental mechanism behind it is the excitation of more low frequency components.

## 4.5.2 Validation of the postulated squat growth process

The monitoring of squats performed by TU Delft on behalf of ProRail provides field data which validates the postulation, see figure 16. More evidence of the validity of the numerical predictions made in annex 1 are provided in annex 3.

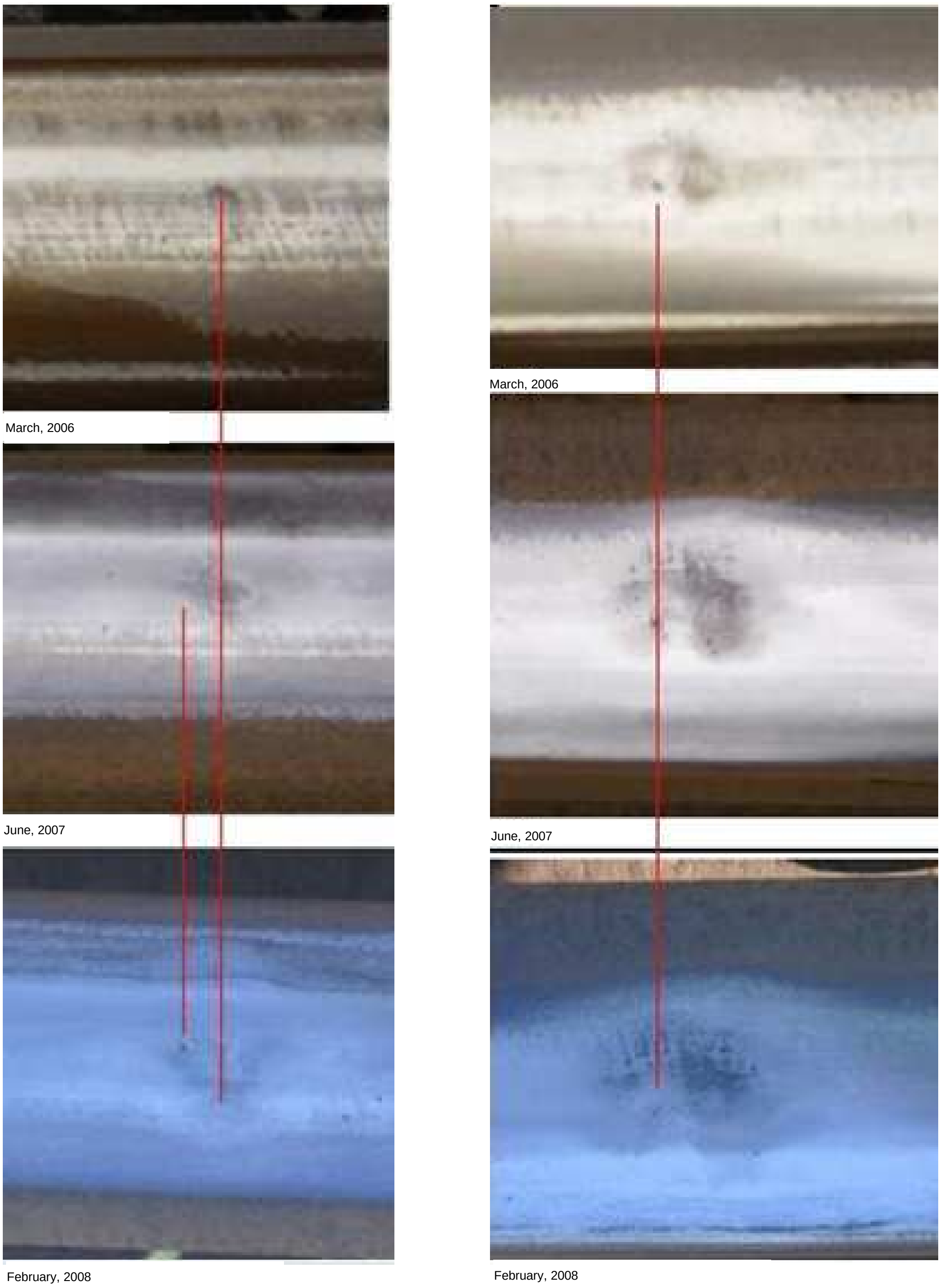


(a) (b)

Figure 16 photos of squats monitored show their growth in agreement with the postulated squat growth process. (a) and (b) show the growth of two squats.

## 4.6 Influential vehicle and track parameters for squat initiation and growth

### 4.6.1 Influence of defect size

It is discussed in sections 4.4 and 4.5, annexes 1, 2 and 4. In particular a critical size for indentations to grow into squats has been derived and validated in annex 4.

### 4.6.2 Influence of traction/braking and unsprung mass

It is observed in the correlation analysis that more squats are found near stations and signals where traction and braking efforts are high. Numerical analysis shows that friction level, hence tangential force plays an important role in the magnitude of von Mises stress and plastic strain. Details are presented in annexes 1 and 4. Validation for annex 1 is in annex 3. Validation for numerical work of annex 4 is contained in 4 itself.

The effect of unsprung mass of vehicle is also investigated. It is found that in the high frequency domain, the unsprung mass on the axle does not result in an extra dynamic load to the first peak force due to lag in wave propagation. On the other hand unsprung mass close to the contact area, such as the mass of the tyre, can lead to a rise in the dynamic force which can be 12 times that of the additional mass. Details are given in annex 5.

### 4.6.3 Influence of welds of continuously welded rails

Welds, both thermite and flash butt, are vulnerable to squats. Out of a field survey of 65 squats, 11 are found at welds, that is 17% of the total. The high percentage of squats at welds may be explained by two main factors: material strength/hardness and longitudinal rail top profile. Analyses of the effects of strength and geometry deviation have been carried out, and the inadequacy of existing standard for weld finish geometry is discussed in annexes 1 and 5.

### 4.6.4 Influence of rail type

Figure 17 shows the effects of two different rail types: 54E1 and 60E1. With all the other conditions being the same, 60E1 has smaller dynamic force for both a large and a small squat.

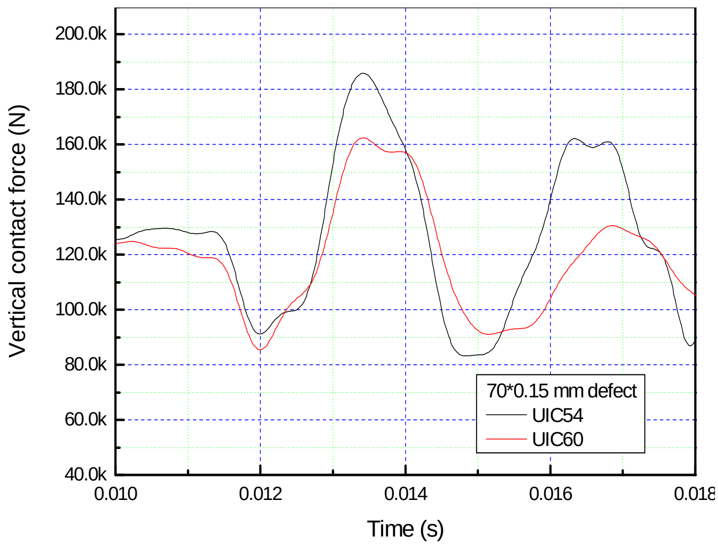


*(a) Dynamic force at a large squat of 70mm long and 0.15mm deep.*

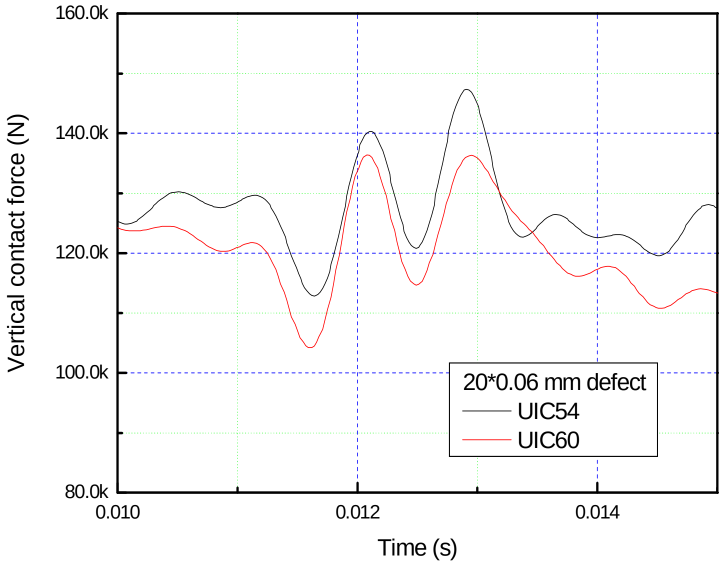


*(b) Dynamic force at a small squat of 20mm long and 0.06mm deep.*

*Figure 17 influence of rail type*

### 4.6.5 Influence of rail grades

Bi-linear elastic-plastic material model is used in this work. The tensile strength of the rail grades are compared with the maximal von Mises stress to determine the propensity of squat initiation and growth, see annexes 1 and 4. From this perspective the higher the material strength is, the higher its resistance to squat initiation and growth. It should be noted that usually material of high strength has also higher wear resistance. Because under certain conditions a proper amount of wear may smooth small geometrical deviation away, the squatting resistance of material might not be accessed only by strength.

## 4.7 Forces and stresses in railpad, sleeper and ballast

The forces and stresses in railpad, sleepers and ballast are discussed in annex 6.

## 4.8 Counter measures

### 4.8.1 Passive counter measures

Class A squats and some class B squats with shallow cracks can be removed effectively by grinding. With severe squats, rail replacement is often inevitable. With each replacement there come 2 new welds, which are disadvantageous. As an alternative a squat can also be repaired by first removing the damaged part of the rail head, and then fill the cavity by welding. This is often applied to parts of switches and crossings. It is very important to guarantee the quality of the welding process and the ensuing grinding to reduce the chance for new squats to occur at the welds.

The large dynamic force at squats causes damages to railpads, fastening, sleepers and ballast. They should also be repaired when squats are removed. Otherwise such track short defects may cause squats to re-appear. It should be pointed out that when grinding the un-uniform sub-surface plastic deformation at the squats due to the local high dynamic force should also be taken into account. Otherwise the remaining in-homogeneity in the surface layer of rail material may promote re-occurrence of squats.

Because squats grow always from small rail top surface defects, preventive and cyclic grinding will greatly reduce their occurrence. Preventive grinding should be applied shortly after new rail is installed. Interval and depth of cyclic grinding should be determined optimally from life cycle costs point of view, with loading conditions taken into account.

Reducing the width of the heat affected zone of welds to below a critical size should help reduce squats at welds. Such technology has been developed and will be tested outside of InnoTrack.

### 4.8.2 Detection of squats

From maintenance point of view, squats should be detected as early as possible so that predictive and preventive actions can be taken in time.

Currently the most widely employed automatic inspection for squats is ultra-sonic detection. This method detects cracks and it is reliable only when the cracks are more than 5 – 7 mm deep. Such a depth of cracks is often too late for grinding.

Eddy current can detect surface cracks of a depth of about 0.1 – 2.5 mm. Surface defects which do not have cracks can not be found. This concerns a large number of class A squats which does not have detectable cracks yet while they are growing.

Because of the impact between wheel and rail at squats, and the associated wavelength of the dynamic force of 20 – 40 mm, squats should be able to be detectable by instrumented wheel or axle box acceleration. The detection may be based on the characteristic magnitude of the impact force and the frequency components. Discussion with a measurement example is given in Section 5 of annex 3. These methods have the advantage to measure or give indication of the magnitude of the force. The tendency of the squats to grow may therefore be assessed based on measurement. This may lead to much more accurate detection and classification of squats than visual inspection. Those small rail surface defects which tend not to grow can then be excluded from being counted as squats.

### 4.8.3 Preventive measures by design

The best counter measures are always those predictive and preventive based on fundamental understanding of the problems and optimal design of the system. To this end, further researches are needed. As the correlation and numerical analyses have shown that a large amount of squats are related to the short pitch corrugation, research on corrugation and on squatting should join hands. Because there have be strong evidences that occurrence of the short pitch corrugation is in one way or another related to some parameters in the track system, it should be possible that one day the controlling parameters of the short pitch corrugations are identified, and can be controlled by improved design.

# 5. Loading and deterioration due to corrugation

The report has so far dealt with squats. The focus is now turned towards the second topic of the report, namely corrugation. As noted above the phenomena may well be connected (for instance they commonly appear together), however the focus of this study is not to investigate this connection, but rather the detrimental effects of corrugation itself.

The influence of corrugation is studied with respect to vertical contact force magnitudes and induced rolling noise. These two were considered the main concerns in relation to corrugation and thus selected for an in-depth analysis.

## 5.1 Background

Small amplitude undulations (irregularities, roughness, waviness) with wavelengths in the order of 1 – 10 cm on the running surfaces of wheels and rails induce high-frequency vertical wheel–rail contact forces. Consequences of such broad-band excitation are vibrations and rolling noise. In particular, contact forces with high magnitudes are generated in operations with out-of-round wheels and/or on track sections with rail corrugation. In severe cases, it may lead to further degradation of wheels and rails in the form of subsurface initiated rolling contact fatigue (RCF). The focus on subsurface initiated RCF is here a consequence of the focus on vertical load magnitudes, which tend to promote subsurface initiated RCF, mainly in wheels. In contrast high interfacial shear in the wheel–rail interface tends to promote surface initiated RCF.

Results from annual measurements of rail roughness on a high-speed line at Koerle in Germany are shown in Figure 14. Rail roughness was measured over a distance of 1.2 m and roughness levels were evaluated in the wavelength interval 1 – 10 cm. A rapid growth of rail roughness, leading to short-pitch corrugation with a dominating wavelength at 6.3 cm, is observed.

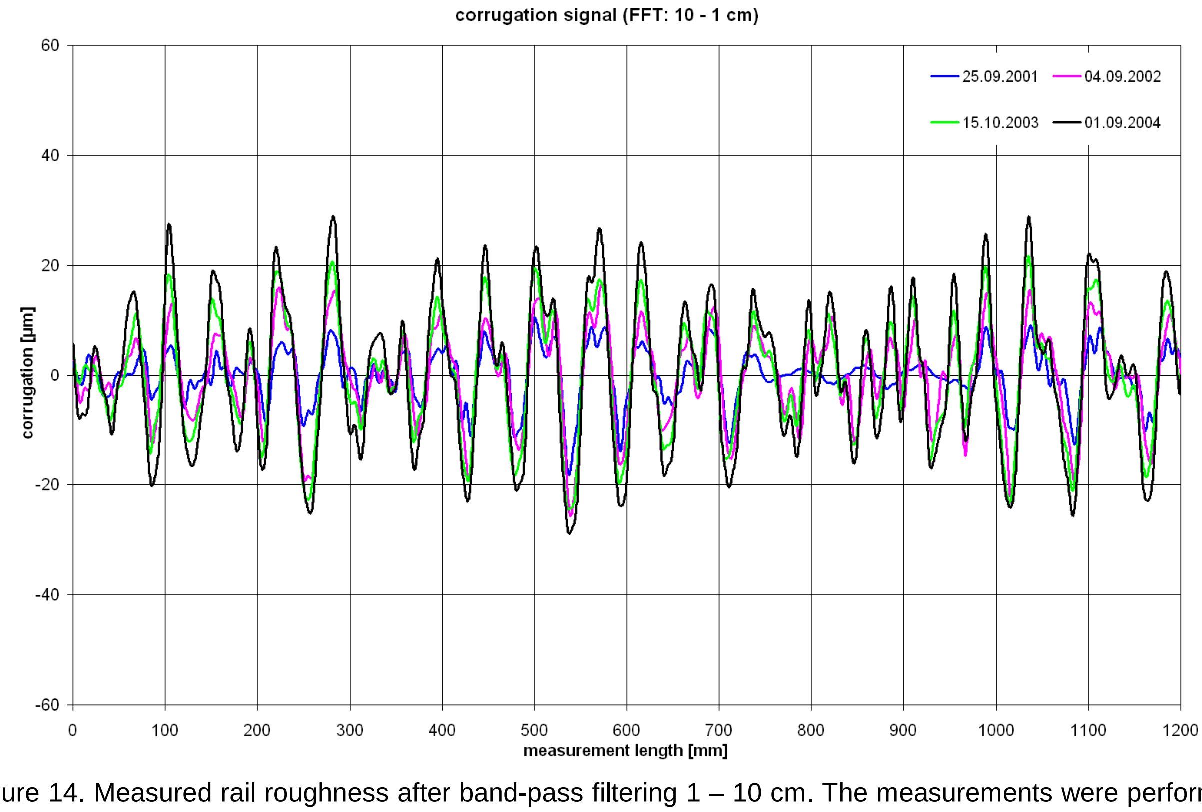


Figure 14. Measured rail roughness after band-pass filtering 1 – 10 cm. The measurements were performed at Koerle in Germany in the autumns of 2001, 2002, 2003 and 2004. From [26].

Vertical wheel–rail contact forces have been measured on an X2 train operating at 200 km/h on the line Stockholm–Gothenburg. The contact forces were recorded using a trailer wheelset instrumented with strain gauges on the wheel discs. Track sections generating high force magnitudes were identified, and it was observed that significant contributions to the contact forces occurred in the frequency range 500 – 1350 Hz. Based on subsequent measurements with the Corrugation Analysis Trolley (CAT), it was confirmed that the rails at these sections were corrugated with roughness levels in the order of 20 dB (re 1 μm) at wavelengths in the interval 4 – 8 cm. This type of corrugation is referred to as short-pitch rail corrugation.

In addition to the rail corrugation, similar roughness may form on wheel treads. In particular tread braking with cast-iron brake blocks is known to generate wheel roughness with similar wavelengths and amplitudes.

The objective of the study was to investigate the influences of train speed and rail roughness level on rolling noise and subsurface initiated RCF impact. Based on the calculated results, a criterion in terms of a limit for acceptable levels of rail roughness can be outlined. The criterion may be used for planning of rail grinding intervals if used together with a system for regular monitoring of roughness levels. The objective is to reduce the generation of RCF and to limit rolling noise levels. The study was based on an integrated analysis using the numerical models in DIFF, FIERCE and TWINS. Here, the computer program DIFF was used to simulate vertical train–track interaction at high frequencies. The FIERCE model was used to predict subsurface initiated RCF impact, while TWINS was used for calculation of rolling noise. Validation of the DIFF and TWINS models were performed by comparison with field tests.

The present Section is an extended summary of the work performed. The full details of the study are given in Reference [27].

## 5.2 Parametric studies

For passenger and freight traffic, a parametric study has been performed to investigate the influences of train speed and rail roughness level on subsurface initiated RCF impact and sound pressure level (SPL). Train–track interaction on tangent track with nominal contact positions on wheel and rail were considered.

Two different values for rail pad stiffness were used, 120 MN/m and 360 MN/m. For the vehicle models in DIFF, different combinations of train speed, axle load, unsprung wheelset mass, wheel radius and axle distance were investigated, see Table 1.

Based on the characteristics of a measured rail roughness spectrum, corresponding to a severely corrugated rail (denoted “Corrugated rail” in the following), rail corrugation spectra of varying severity were generated by adding or subtracting multiples of 3 dB from the original spectrum in the wavelength interval 4 – 8 cm, see Figure 15. For longer and shorter wavelengths, roughness levels were increased or reduced between 0 and 2.5 dB to maintain the shape of the new spectra as compared to the measured spectrum.

Table 1. Input data for vehicle models in DIFF

| Vehicle model | | Train speed [km/h] | Axle load [tonnes] | Unsprung mass [kg] | Wheel radius [m] | Axle distance [m] |
|---|---|---|---|---|---|---|
| Passenger | 1 | 150 – 300 | 17 | 1200 | 0.44 | 2.9 |
| | 2 | 150 – 300 | 17 | 1900 | 0.55 | 2.9 |
| Freight | 1 | 60 – 120 | 22.5 | 1200 | 0.44 | 1.8 |
| | 2 | 60 – 120 | 30 | 1200 | 0.44 | 1.8 |

A quantification of rail corrugation in the wavelength interval 3 – 8 cm is suggested by taking the mean square of rail roughness levels in the five 1/3 octave bands with centre wavelengths 3.16, 4.0, 5.0, 6.3 and 8.0 cm as

$$\tilde{r}^2_{\mathrm{mean,\,3\text{-}8\,cm}} = \tilde{r}^2_{\mathrm{ref}} \frac{1}{5} \sum_{i=1}^{5} 10^{L_{\mathrm{r},i}/10} \,. \tag{1}$$

The corresponding mean roughness level $L_{\mathrm{r,\,3\text{-}8\,cm}}$ is obtained as

$$L_{\mathrm{r,\,3\text{-}8\,cm}} = 20\log_{10}\left(\frac{\tilde{r}_{\mathrm{mean,\,3\text{-}8\,cm}}}{r_{\mathrm{ref}}}\right) \text{ [dB re 1 µm]}. \tag{2}$$

The mean roughness levels for the “Corrugated rail” and the ISO 3095 [28] spectra are 17.7 dB and 4.0 dB (re 1 µm), respectively, see the legend in Figure 15. The mean roughness levels for the generated spectra are obtained by adding or subtracting the corresponding multiples of 3 dB from the mean roughness level of the “Corrugated rail”.

In the DIFF simulations with a passenger vehicle model, rail roughness level spectra with wavelengths in the interval 2 – 250 cm were accounted for. This corresponds to a broad-band excitation in the frequency range 17 – 4200 Hz at train speeds in the interval 150 – 300 km/h. For the freight vehicle simulations, wavelengths in the interval 1 – 250 cm were studied corresponding to excitation in the range 7 – 3300 Hz at train speeds 60 – 120 km/h. Levels according to the ISO 3095 spectrum were assumed for wavelengths $\lambda_k$ > 16 cm. Measured wheel roughness level spectra were used for the freight (with cast iron tread brakes) and passenger (with disc brakes) vehicle models, respectively. In each DIFF simulation, the effective wheel–rail roughness spectrum calculated as the energetic sum (sum of mean squares) of wheel and rail roughness was used as input.

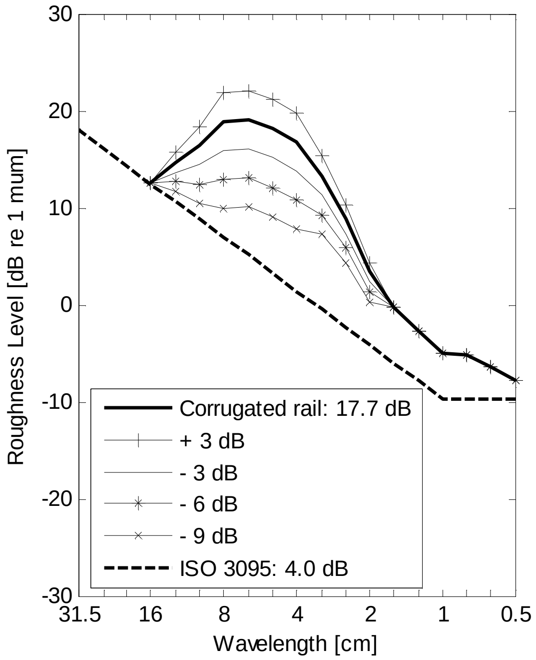


Figure 15. Rail roughness level spectra used in the parametric studies

## 5.3 Subsurface initiated rolling contact fatigue

For the computer program FIERCE, an index for subsurface initiated rolling contact fatigue was derived from the Dang Van equivalent stress. The index can be expressed as

$$FI_{\text{sub}} = \frac{F_z}{4\pi ab}(1+\mu^2) + a_{\text{DV}}\sigma_{\text{h, res}} \,. \tag{3}$$

Here $F_z$ is the vertical wheel–rail contact force, $a$ and $b$ the hertzian contact semi-axes, $a_{\text{DV}}$ a material parameter and $\sigma_{h,res}$ the hydrostatic part of the residual stress (positive in tension).

The traction coefficient $\mu$ is given by

$$\mu = \frac{\sqrt{F_x^2 + F_y^2}}{F_z} \,, \tag{4}$$

where $F_x$ and $F_y$ are the longitudinal and lateral wheel–rail contact forces, respectively. For $\mu$ larger than roughly 0.3, the maximum shear stress will occur in the surface. This will result in surface initiated RCF (and wear). Since the current study focuses on the influence on subsurface initiated RCF, these situations are not of interest. This motivates the neglected influence of traction/braking in the current study, which for situations of $\mu < 0.3$ would lead to a maximum reduction of $FI_{\text{sub}}$ in the order of 10%.

Fatigue is predicted if $FI_{\text{sub}}$ exceeds the material's fatigue limit in shear (reduced due to the occurrence of material defects). A typical reduced value is 220 MPa. This roughly corresponds to the presence of a material defect with a characteristic dimension of 1 mm, which is in line with regulations for wheel material cleanliness.

The 95$^{\text{th}}$ percentile of $FI_{\text{sub}}$ was adopted to quantify the fatigue impact. The motivation is that $FI_{\text{sub}}$ relates to the fatigue limit of the material, which in turn corresponds to about 1 to 10 million load cycles (in our case wheel passages). Consequently, adopting the peak magnitude of $FI_{\text{sub}}$ as a representative measure would be very conservative. On the other hand, adopting the mean value of $FI_{\text{sub}}$ would show no effect of the corrugation at all. Although somewhat arbitrary, the 95$^{\text{th}}$ percentile was considered a suitable compromise between these two extremes. It should be kept in mind that there exist both systematic and random variations in vehicle and track characteristics not accounted for in the current study that will cause the seemingly deterministic 95$^{\text{th}}$ percentile to show operational variations.

For each combination of vehicle model, train speed and mean rail roughness level, the 95$^{\text{th}}$ percentile of the subsurface initiated RCF impact was calculated. Figures 16(a,b) illustrate the results for passenger vehicle model 1 and rail pad stiffness 120 MN/m in two alternative formats: surface plot and contour plot. As expected, RCF impact is seen to increase with increasing train speed and increasing rail roughness. From Figure 3(b), it can be observed that the 95$^{\text{th}}$ percentile of $FI_{\text{sub}}$ is close to 220 MPa at train speed 200 km/h if the track contains short-pitch rail corrugation with a rail roughness level spectrum corresponding to the "Corrugated rail" in Figure 2 (with $L_{\text{r, 3-8 cm}}$ = 17.7 dB).

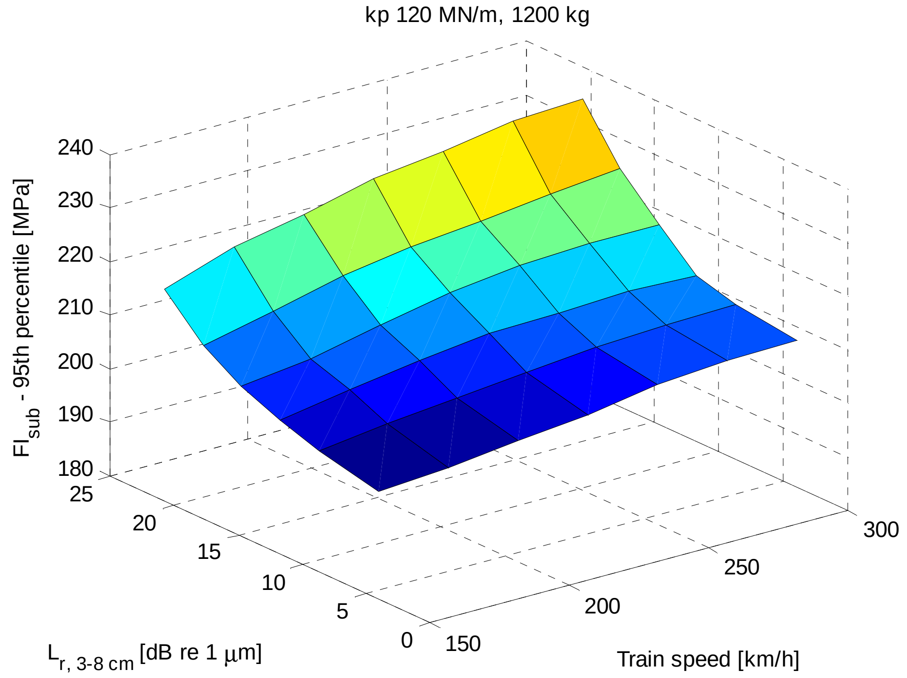


Figure 16(a). Surface plot illustrating the calculated influences of train speed and mean rail roughness level (wavelength interval 3 – 8 cm) on the 95th percentile of subsurface initiated RCF impact. Passenger vehicle model 1 (see Table 1). Rail pad stiffness 120 MN/m

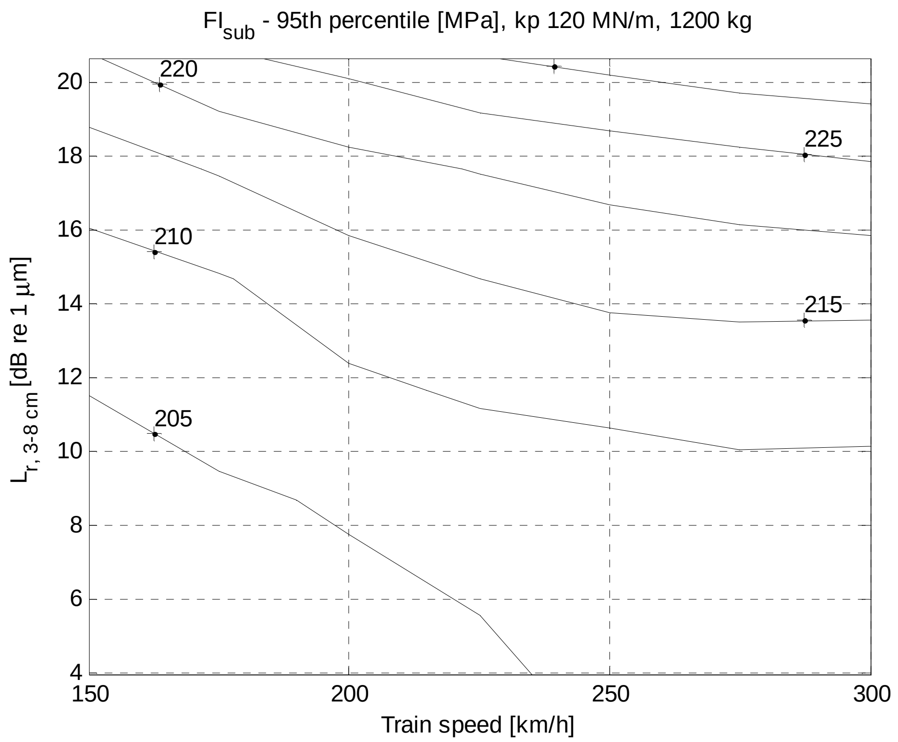


Figure 16(b). Contour plot illustrating the calculated influences of train speed and mean rail roughness level (wavelength interval 3 – 8 cm) on the 95th percentile of subsurface initiated RCF impact. Passenger vehicle model 1 (see Table 1). Rail pad stiffness 120 MN/m

## 5.4 Rolling noise

TWINS was used to calculate SPL at 7.5 m from track centre, $L_{\mathrm{p}}^{7.5\mathrm{m}}$, for different combinations of train speed and effective wheel–rail roughness level spectrum. Investigated train speeds were in the interval 60 – 275 km/h. For these speeds, rolling noise is generally regarded as the dominant source of railway noise. The calculated influences of train speed *v* and mean rail roughness level $L_{\mathrm{r,\,3\text{-}8\,cm}}$ on SPL are shown as contour plots in Figure 17.

Based on least square fitting of the calculated SPLs, response surface models were determined to quantify the effects of train speed and mean rail roughness level according to

$$\text{Passenger: } L_{\mathrm{p}}^{7.5\,\mathrm{m}} = 94.4 + 28.6\log_{10}\left(\frac{v}{200}\right) + 0.9L_{\mathrm{r,\,3\text{-}8\,cm}} \text{ [dB(A)]}, \tag{5}$$

$$\text{Freight: } L_{\mathrm{p}}^{7.5\,\mathrm{m}} = 95.7 + 34.9\log_{10}\left(\frac{v}{100}\right) + 0.3L_{\mathrm{r,\,3\text{-}8\,cm}} \text{ [dB(A)]}. \tag{6}$$

For passenger traffic at a given train speed, it is observed in Equation (5) that an increase in mean rail roughness level $L_{\mathrm{r,\,3\text{-}8\,cm}}$ nearly leads to a corresponding one-to-one increase (factor 0.9) in SPL. This is because roughness on X2 trailer wheels is negligible compared to the investigated levels of rail roughness. For freight traffic, the increase in SPL with increasing rail roughness is not as significant since the freight wheels themselves have considerable roughness levels. Thus, rail grinding to reduce rolling noise is not as efficient for freight traffic as it is for passenger traffic. For freight traffic, the influence of train speed is more significant.

As an example, it can be concluded from Figure 17 that X2 passenger traffic on a “Corrugated rail” (with $L_{\mathrm{r,\,3\text{-}8\,cm}}$ = 17.7 dB) generates a rolling noise level of 110 dB(A) at 200 km/h. If the rails could be maintained to not exceed the ISO 3095 spectrum ($L_{\mathrm{r,\,3\text{-}8\,cm}}$ = 4.0 dB), a 12 dB reduction to 98 dB(A) seems possible. For a given mean rail roughness level, increasing the train speed from 200 km/h to 250 km/h would result in about a 3 dB increase in SPL.

## 5.5 Discussion

The influences of train speed and mean rail roughness level in wavelength interval 3 – 8 cm on subsurface initiated RCF impact and rolling noise have been determined for freight and passenger traffic on a track with 60E1 rails, resilient rail pads and concrete sleepers on ballast. For passenger traffic, it was shown that the risk for subsurface initiated RCF is small unless the rails/wheels are severely corrugated. Increasing axle loads to 30 tonnes leads to significant RCF impact even on smooth rails. In operations, this is addressed by the introduction of conformal rail/wheel profiles to increase the contact patch size. The annoyance due to rolling noise may be significant in populated areas even for moderate levels of rail roughness. Based on the presented results, a criterion for a maximum allowed mean rail roughness level in the wavelength interval 3 – 8 cm can be determined. Different criteria can be used for different track sections depending on population density, type of traffic and train speed. If the mean rail roughness level for a given track section exceeds the accepted level, grinding of the rails is required.

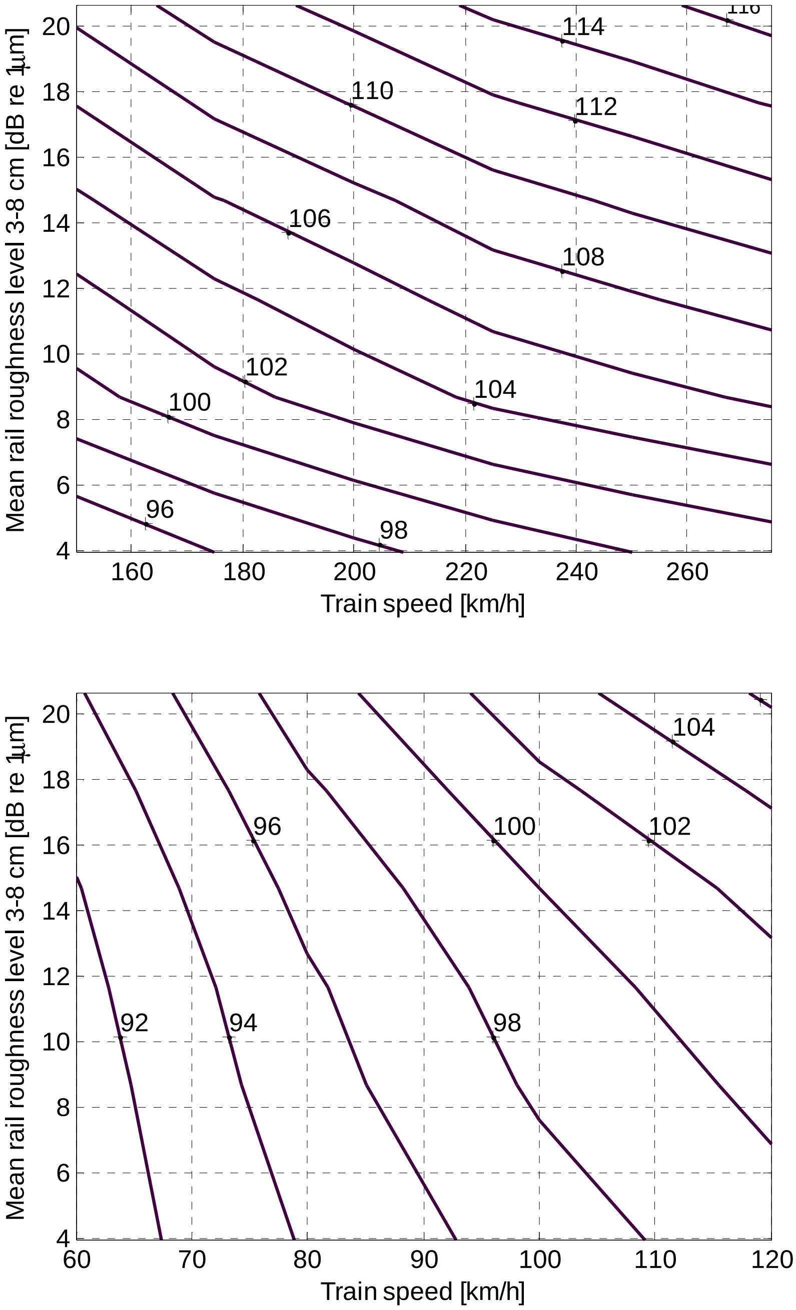


Figure 17. Contour plots illustrating the influence of train speed and mean rail roughness level on SPL [dB(A)] at 7.5 m from track centre: (upper) X2 train with disc-braked trailer wheelsets, (lower) freight vehicle with SJ57 wheelsets and cast-iron brake blocks. Track with 60E1 rails, resilient rail pads and concrete monobloc sleepers on ballast

# 6. Conclusions

The current report focuses on two phenomena: squats and corrugation.

Regarding squats, correlation analyses were first carried out to clarify globally the phenomena and operation conditions related to squats. A hybrid multibody-finite element model was accordingly developed and applied to the analyses of the initiation and growth of squats, and to the identification of the most influential parameters of squatting. A growth process of squats was postulated based on numerical simulation, and was subsequently validated by field monitoring. Further a critical size for small rail top geometrical defects to grow into squats has been derived and validated. This critical size may be directly applied to visual inspection and classification of squats so that false reporting of squats can be avoided. The critical size can be applied as a minimum action rule for preventive or early corrective maintenance actions, such as rail grinding. The analyses have been performed for the Dutch situations, but the validated model and the established methodology can be applied to any other operational conditions. The model may also have the capability to relate the severity of some track short defects quantitatively to some measurement of the dynamic wheel-rail interaction at the defects so that automatic detection of the defects at their early stage is possible. Finally corrective and preventive measures against squats are discussed.

# 7. References

[1] P. Clayton, Tribological aspects of wheel-rail contact: a review of recent experimental research, Wear 191 (1996) 170-183.
[2] R. Nakumura, S. Owaku and N. Enomoto, The rail shelly crack in Japan, Q. Rep. Railway Tech. Res. Inst. Jpn. National Railways, 6 (3) (1965) 34-44.
[3] A. Ito and R. Kurihara, Shelling of rails experienced in Japanese railways, Bull. Permanent Way Sot. Jpn., 13 (1 and 8) (1965) 17-32.
[4] P. Clayton and M.B.P. Allery, Metallurgical aspects of surface damage problems in rails, Can. Metall. Q., 21 (1) (1982) 31-46.
[5] R. Deroche, J.P. Bettembourg, B. Prasil, J.P. Bertrand and C. Juckum, Rolling contact fatigue cracks on SNCF conventional tracks, in J.J. Kalker (ed.), Rail Quality and Maintenance for Modern Railway Operation, Kluwer, Dordrecht, 1993, pp. 435-448.
[6] J. Smulders, Management and research tackle rolling contact fatigue, Railway Gazette International, June 2003, 439 – 442.
[7] UIC Code 712, Rail defects, 4th edition, January 2002.
[8] P. Clayton, M.B.P. Allery and P.J. Bolton, Surface damage phenomena in rails, J. Kalousek R.V. Dukkipati and G.M.L. Gladwell (Ed). Proceedings of the conference on Contact Mechanics and Wear of Rail/wheel Systems, Vancouver, British Columbia, July 6-9, 1982, 419-443, University of Waterloo Press, 1983.
[9] P. Clayton and D.N. Hill, Rolling contact fatigue of a rail steel, G.M.L. Gladwell, H. Ghonem and J. Kalousek (Ed). Proceedings of the conference on Contact Mechanics and Wear of Rail/wheel Systems II, University of Rhode Island, Kingston, R.I., July 8 - 11, 1986, 361-378, University of Waterloo Press, 1987.
[10] D.F. Cannon, H. Pradier, Rail rolling contact fatigue – Research by the European Rail Research Institute, Wear 191 (1996) 1-13.
[11] S. Bogdanski, M. Olzak, J. Stupnicki, Numerical stress analysis of rail rolling contact fatigue cracks, Wear 191 (1996) 14-24.
[12] S. Bogdanski and R. Lewicki, 3D Model of Entrapped Liquid in Rolling Contact Fatigue Cracks in Rails, Wear 265 (2008), 1356 – 1362.
[13] K Kondo, K. Yoroizaka and Y. Sato, Cause, increase, diagnosis, countermeasures and elimination of Shinkansen shelling, Wear 191 (1996) 199-203.
[14] M. Ishida, M. Akama, K. Kashiwaya and A. Kapoor, The current status of theory and practice on rail integrity in Japanese railways – Rolling contact fatigue and corrugations, Fatigue Fract Engng Mater Struct 26, 909-919, 2003.
[15] P. E. Bold, M. W. Brown and R. J. Allen, Shear mode crack growth and rolling contact fatigue, Wear 144 (1991) 307-317.
[16] R. Smallwood, J. C. Sinclair and K. J. Sawley, An optimization technique to minimize rail contact stresses, Wear 144 (1991) 373-384.
[17] M. Busquet, L. Baillet, C. Bordreuil and Y. Berthier, 3D finite element investigation on the plastic flows of rolling contacts—correlation with railhead microstructure observations, Wear 258 (2005) 1071–1080.
[18] K. Dang Van and M.H. Maitournam, Rolling contact in railways: modelling, simulation and damage prediction, Fatigue Fract Engng Mater Struct 26 (2003), 939-948.
[19] Rail Damages, the Blue Book of RailTrack, February, 2001, UK.
[20] Classification of Squats explained with examples, Squat handout, ProRail, version 2, March 2004 (in Dutch)
[21] A. F. Bower and K. L. Johnson, Plastic flow and shakedown of the rail surface in repeated wheel-rail contact, Wear, 144 (1991) 1-18.
[22] D.F. Cannon, K.-O. Edel, S.L. Grassie and K. Sawley, Rail defects: an overview, Fatigue Fract Engng Mater Struct 26 (2003), 865 – 887.
[23] Li, Z, Correlation Analysis of Squats, Internal project report, Railway Engineering group, TU Delft, 5 March, 2006
[24] Kalousek, J and Grassie, S.L. (2000), Rail corrugation: causes and cures, Int. Railway J. (July) 24–26.
[25] Zhao X., Li, Z., Esveld, C., and Dollevoet, R., The Dynamic Stress State of the Wheel-Rail Contact. WSEAS Transactions on Applied and Theoretical Mechanics, Issue 2, Volume 2, February 2007, ISSN: 1991-8747 pp 52 – 59

[26] R. Heyder, Deutsche Bahn AG Germany, Private communication, 2009
[27] J.C.O. Nielsen and A. Ekberg, Subsurface initiated rolling contact fatigue and rolling noise – influence of train speed and rail roughness, Research report 2009:04, Department of Applied Mechanics, Chalmers University of Technology, Gothenburg, Sweden, 26 pp
[28] CEN/TC256, Railway applications – acoustics – measurements of noise emitted by railway vehicles. Preliminary European norm prEN 3095, September 2003, 35 pp

# 8. Annexes

[1] Z. Li, X. Zhao, C. Esveld, R. Dollevoet and M. Molodova, *An Investigation into the Causes of Squats – Correlation Analysis and Numerical Modelling*, Wear 265 (2008) 1349 – 1355, doi:10.1016/j.wear.2008.02.037

[2] Z. Li, X. Zhao, R. Dollevoet and M. Molodova, Differential Wear and Plastic Deformation as a Cause of Squat at Track Local Stiffness Change Combined with Other Track Short Defects, Vehicle System Dynamics, Vol.46, Sup. 2008, 237-246, DOI: 10.1080/00423110801935855

[3] Z. Li, X. Zhao, M. Molodova and R. Dollevoet: The validation of some numerical predictions on squats growth, Proceedings 8th International Conference on Contact Mechanics and Wear of Rail/Wheel Systems, Florence, Italy, 15 – 18 September, 2009, pp. 369 - 378, ISBN: 978-88-904370-0-7

[4] Z. Li, X. Zhao, and R. Dollevoet, The determination of a critical size for rail top surface defects to grow into squats, Proceedings of the 8th International Conference on Contact Mechanics and Wear of Rail/Wheel Systems, Florence, Italy, 15 – 18 September, 2009, pp. 379 – 388, ISBN: 978-88-904370-0-7.

[5] Z. Li, X. Zhao, C. Esveld, and R. Dollevoet, , *Rail Stresses, Strain and Fatigue under Dynamic Wheel-Rail Interaction*. Proceedings International Heavy Haul Conferences 2007 Specialist Technical Session, June 11 – 13, 2007 at Kiruna, Sweden, 389 - 396 (ISBN: 978-91-633-0607-5)

[6] Z. Li and X. Zhao, The dynamic vertical forces on and stresses in railpad, sleepers and ballast cause by a severe squat, TU Delft, 28 Feb. 2009.

[7] J.C.O. Nielsen and A. Ekberg, Subsurface initiated rolling contact fatigue and rolling noise – influence of train speed and rail roughness, Research report 2009:04, Department of Applied Mechanics, Chalmers University of Technology, Gothenburg, Sweden, 26 pp